Discontinuous Galerkin Method on Unstructured Hexahedral Grids for 3D Euler and Navier-Stokes Equations

Charles Hirsch*
Numeca Int., Brussels Belgium

Andrey Wolkov†
TsAGI, Moscow, Russia

and

Benoit Leonard‡
Numeca Int., Brussels Belgium

A Finite-Element Discontinuous Galerkin Method (DGM) has been developed for 3D Euler and Navier-Stokes equations, on unstructured hexahedral grids. Specific features related to the DGM implementation, up to fourth order accuracy, including the treatment of curved boundaries are described.
In order to accelerate the convergence of the algorithm, both agglomeration and p-multigrid strategies have been implemented, relying on implicit and explicit smoothers.
The algorithm has been validated and evaluated in terms of CPU and memory performance on several reference cases, such as analytical 3D convection solutions, the flow around a cylinder, a flat plate, as well as for a 3D acoustic propagation problem. Applications are presented for the 3D turbulent flow on an isolated wing and compared with a standard second-order finite-volume method.

I. Introduction

It is generally recognized that unstructured hexahedral grids offer significant advantages on tetrahedral grids, and the object of this paper is to present the development and application of the DGM on unstructured hexahedral grids, for .3D Euler and Navier-Stokes equations. One of the challenges of the DGM-approach for three-dimensional problems is to minimize the required computer memory and CPU cost. Computations of three-dimensional integrals, inherent in this method, have been carried out using the Quadrature-Free approach proposed by Atkins and Shu.

II. Governing equations

The DGM is applied to the system of Navier-Stokes equations in conservative form:

$$\frac{\partial U}{\partial t} + \vec{\nabla} \cdot \left(\vec{F} - \vec{F}_V \right) = q \tag{1}$$

where U represents the conservative variables, F and Fv are respectively the inviscid and viscous fluxes. The Navier-Stokes equations are rewritten for the primitive variables Q=(ρ,u,v,w,p), as follows:

$$\Gamma \frac{\partial Q}{\partial t} + \vec{\nabla} \cdot \left(\vec{F} - \vec{F}_V \right) = q \tag{2}$$

where $\Gamma = \partial U / \partial Q$.

The numerical solution is represented in each element by linear combinations of basic functions: $\varphi_i(\vec{x})$

$$U(t, \vec{x}) = \sum_{j=1}^{Kf} u_j(t) \varphi_j(\vec{x}) \tag{3}$$

* Professor, NUMECA Int., Brussels, Belgium; charles.hirsch@numeca.be; AIAA member
† TsAGI, Moscow, Russia; wolkov@progtech.ru
‡ Head of Unstructured CFD group, NUMECA Int., Brussels, Belgium; benoit.leonard@numeca.be

where $u_j(t)$ are the expansion coefficients to be defined, Kf is the number of basis functions of maximum order of polynomial K, as follows

$$Kf = \frac{(K+1)(K+2)(K+3)}{6} \tag{4}$$

In the present investigation K is defined from 0 up to 2, and Kf ranges from 1 up to 10. Note that the order of accuracy of the resulting DGM scheme is (K+1).
The basis functions are polynomials and their set is defined as follows:

$$\varphi_0 = 1, \quad \varphi_1 = (x - x_0), \quad \varphi_2 = (y - y_0), \quad \varphi_3 = (z - z_0), \quad \varphi_4 = (x - x_0)^2, \quad \varphi_5 = (y - y_0)^2,$$
$$\varphi_6 = (z - z_0)^2, \ \varphi_7 = (x - x_0)(y - y_0), \ \varphi_8 = (x - x_0)(z - z_0), \ \varphi_9 = (y - y_0)(z - z_0) \tag{5}$$

where x_0, y_0, z_0 is the central point of the hexahedral cell.

According to the standard Galerkin finite-element formulation the residual of the governing equations is formulated in the weak form obtained by multiplying the residual by each trial function ϕ_i (i=1,…,Kf) and integrating by parts over each element E, leading to

$$\frac{d}{dt}\int_{\Omega^E} \varphi_i \, \Gamma Q d\Omega + \oint_{S^E} \varphi_i \left(\vec{F} - \vec{F}_V\right) \cdot d\vec{S} - \int_{\Omega^E} \vec{\nabla}\varphi_i \left(\vec{F} - \vec{F}_V\right) d\Omega_E = 0 \tag{6}$$

Equation (6) contains volume integrals and an integral over the control volume faces. The main difficulty is to calculate this surface integral. The basis functions are discontinuous on the cell faces between different elements and as a consequence the fluxes are discontinuous also. The inviscid flux at the cell face is therefore obtained by an approximate Riemann solution, defined by the standard Roe upwind numerical flux:

$$\vec{F}_{face} \cdot d\vec{S} = \frac{1}{2}(\vec{F}^L + \vec{F}^R) \cdot d\vec{S} - \frac{1}{2}|A|\left(U^L - U^R\right) \tag{7}$$

where A is the Jacobian of the inviscid flux: $A = \dfrac{\partial(\vec{F} \cdot d\vec{S})}{\partial U}$.

The viscous flows at cell faces are defined by simple averaging. However, as they contain the gradients of the discontinuous solution, a specific procedure has to be applied., for instance by developing separately the flow variable gradients as linear combinations of the basis functions, and solving for the coefficients. Writing

$$\frac{\partial Q}{\partial x_i}(t, \vec{x}) = \sum_{j=1}^{Kf} G_{i,j}(t) \, \varphi_j(\vec{x}) \qquad i = 1, 2, 3 \tag{8}$$

After multiplying these equations by the trial functions ϕ_i and integrating by parts over each element E we obtain the following system for the unknown G_i coefficients

$$\int_{\Omega^E} \sum_{j=1}^{Kf} G_{i,j}\varphi_j \, \varphi_k \, d\Omega + \oint_{S^E} \varphi_k Q(\vec{n}_i \cdot d\vec{S}) - \int_{\Omega^E} \frac{\partial \varphi_k}{\partial x_i} Q d\Omega = 0 \qquad i = 1, 2, 3 \quad k = 1, ..., Kf \tag{9}$$

The system of non-linear equations for the determination of the expansion coefficients has been obtained after assuming a constant transformation matrix Γ within each cell:

$$\frac{dq_j}{dt} = -\Gamma^{-1} M^{-1} \left[\oint_{S^E} \varphi_j \left(\vec{F} - \vec{F}_V\right) \cdot d\vec{S} - \int_{\Omega^E} \vec{\nabla}\varphi_j \left(\vec{F} - \vec{F}_V\right) d\Omega \right] \tag{10}$$

This forms a system of ordinary differential equations (ODE) in time, which has to be integrated by an appropriate method, discussed in section IV.

III. Flux Calculation

Accurate evaluations of both volume and surface integrals are required and this is achieved through Gauss point integration. The optimal distribution of Gauss points for volume and surface integrals is available only for elementary configurations – triangle, tetrahedron, etc. For hexahedral cells, each side of the control volume has been divided into two triangles, the control volume being decomposed in 12-tetrahedra. When such division results in

cells of negative volume, the face is divided into four triangles with the central point located in the gravity center of the face.

On the other hand, the nonlinearity of the fluxes leads to products of variables, each one being decomposed according to equation (3), with a very costly evaluation in terms of arithmetic operations. This can be significantly improved following the Quadrature-Free (Q-F) approach of Atkins and Shu[13], based on a decomposition of the fluxes on the same basis function space, as follows

$$f(U) = \sum_{j=1}^{Kf} f_j \, \varphi_j \tag{11}$$

More details will be given in the full paper.

IV. Time Integration

The time integration is performed by an explicit Runge-Kutta method that provides required high order of accuracy. Different R-K strategies were considered and a 5-stage R-K approach was used to increase the stability limits.

More details will be given in the full paper.

V. Multigrid Convergence Acceleration

The multigrid method (MG) is essential for achieving high convergence accelerations and is widely used both on structured as well as unstructured grids. On structured grids the multigrid technique consist in defining a series of coarser grids by removing every second line in each direction, definition hereby an optimal ratio of grid points between successive grids of 8. This is much more difficult to achieve on unstructured grids where either a remeshing technique is required or alternatively an agglomeration method whereby cells are agglomerated into polyhedral structures with an arbitrary number of faces. This approach has been extended to unstructured hexahedral grids and implemented together with a p-multigrid approach.

The details of the implementation will be presented in the full paper.

The application and convergence acceleration obtained with the DGM agglomeration multigrid is shown for the test cases described in the following section, namely the cylinder, the flat plate and the 3D wing.

A. The 2D inviscid potential flow around a cylinder

Calculations of the inviscid flow around a circular cylinder is performed on 2D grid containing 12950 cells. Fragments of this grid are shown on Figure 1, which displays two agglomerated grid levels and the convergence history with and without the agglomeration multigrid option. Based on 3 multigrid levels, the residuals history clearly shows the performance gain from the multigrid method.

Figure 1: Agglomerated grids and convergence history comparison between single (green) and multigrid (red) calculations for the inviscid cylinder flow case

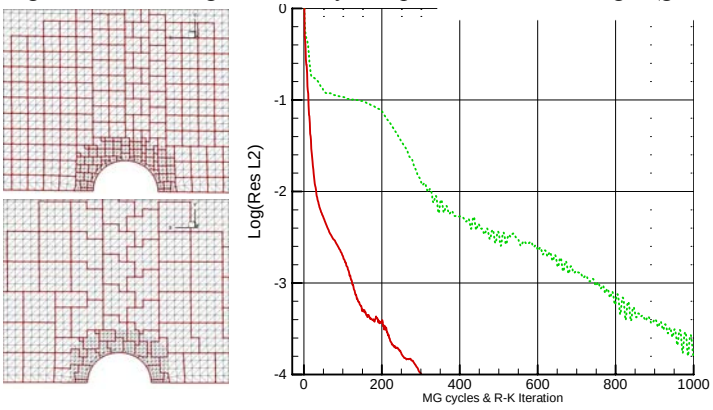

B. Laminar flat plate flow

The laminar flow on a flat plate was considered in the computational region -0.24<X<0.4, 0<Y<0.05. The plate is located in the interval 0<X<0.4. Calculations were performed using a 3-level agglomerated multigrid with recalculation of viscous flux at the first and the second stages. Figure 2 shows the obtained convergence acceleration, with a CPU gain of a factor close to 6.

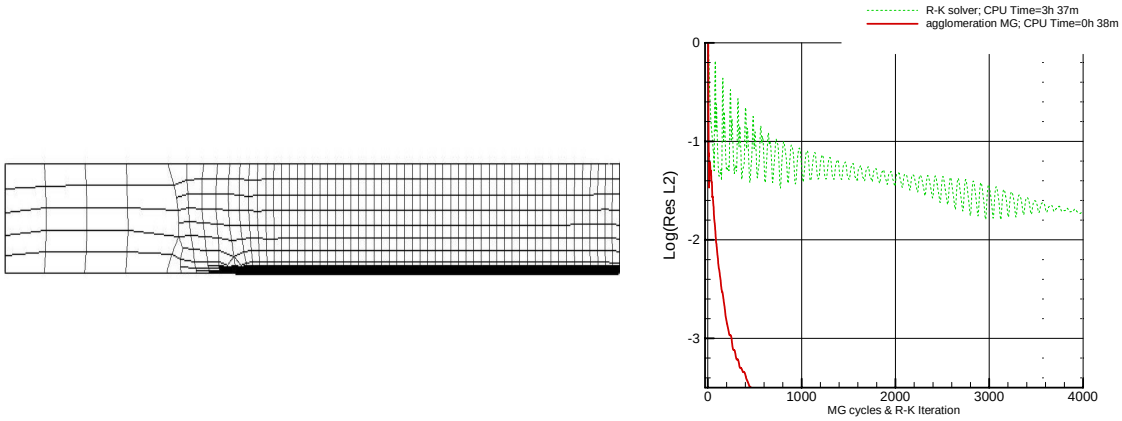

Figure 2: Mesh and convergence acceleration for 3-level agglomerated multigrid (red), compared to a single grid (green) calculation

C. 3D Turbulent flow around the LANNN wing

Two series of calculations were performed for LANN wing at a Reynolds number of 7.17 10^6, incident M=0.4, α=0.6 deg, with a 3-level multigrid and recalculation of viscous flux at the first stage only. The Spalart-Allmaras turbulent model is applied. The finest grid corresponds to 420000 degrees of freedom.

This test case compares the DGM solution with a standard finite volume second order solution on unstructured hexahedral grids, with agglomeration multigrid, for similar number of DOF's, with the Spalart-Allmaras turbulence model. The comparative calculations have been carried out for the LANN wing on unstructured hexahedral grids generated by the HEXPRESS™ grid generator form NUMECA, with 190213 cells (DG approach) and with 625076 cells (F-V approach), with first mesh point locations above the solid boundaries of the order of $y_+ \approx 1$. Parts of the mesh are shown on figure 3.

The incident flow conditions are M=0.4, α=0.6º, Re=7.17 million.

Comparisons of pressure distribution for three wing sections are shown on figure 9, at z=0.02 (root section), z=0.5 (mid-span section) and z=0.98, close to the tip section, for the FV and DGM solution, the latter on a 3 times coarser grid. The two methods provide nevertheless approximately the same results.

Other results for higher order methods will be shown in the final paper

VI. Conclusions

The Discontinuous Galerkin Method (DGM) has been developed for 3D Euler and turbulent Navier-Stokes flows on unstructured hexahedra, up to fourth order accuracy in association with Runge-Kutta explicit time integration, as well as an implicit time integration as smoother associated to agglomeration multigrid, coupled to p-multigrid.

When compared to standard second order finite volume schemes, the DGM shows improved accuracy on grids with the same number of degrees of freedom (DOF).

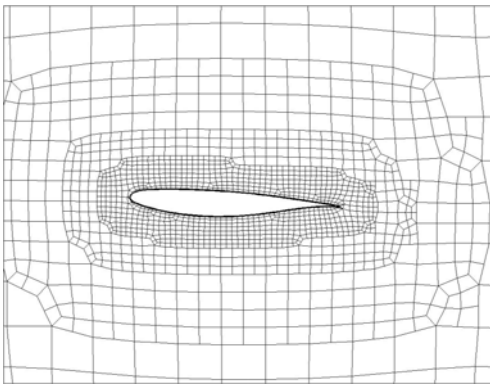

Unstructured hexahedral grid on LANN wing

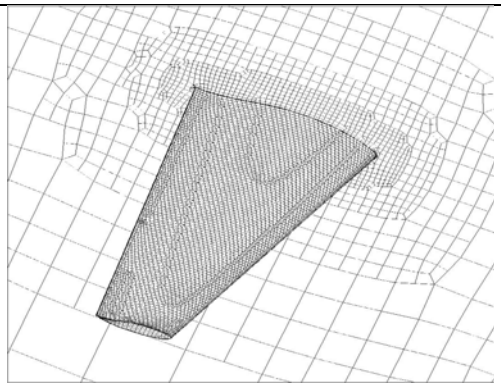

Unstructured hexahedral grid on LANN wing

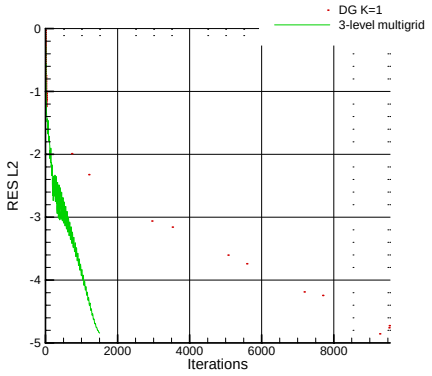

Convergence history for the DGM, K=1 case.

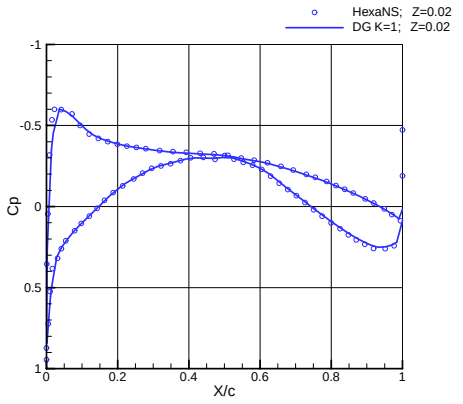

Comparison of pressure coefficients between the FV (points) and DGM (line), at root section z=0.02

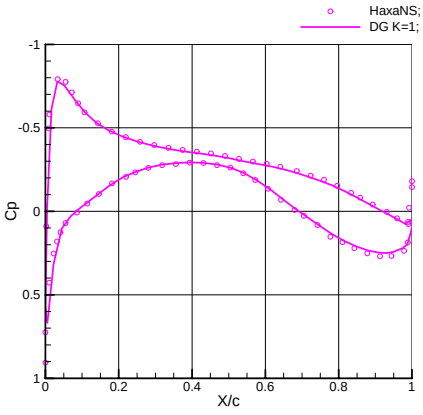

Comparison of pressure coefficients between the FV (points) and DGM (line), at mis-span section z=0.5

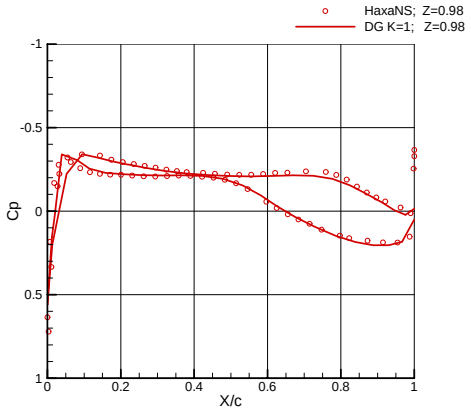

Comparison of pressure coefficients between the FV (points) and DGM (line), at tip section z=0.98

Figure 3: Turbulent computation on the LANN wing, with FV and DGM methods on grids with similar number of DOF's.